Basal-Plane Orientation of Zn Electrodeposits Induced by Loss of Free Water in Concentrated Aqueous Solutions

Shota Inoguchi, Atsushi Kitada,[z] Kazuhiro Fukami,[*] and Kuniaki Murase[*]

Department of Materials Science and Engineering, Kyoto University, Kyoto 606-8501, Japan

Concentrated aqueous solutions attract considerable attention because water electrolysis can be suppressed due to a decrease in the amount of free water. The present study focuses on electrodeposition behaviors of metallic zinc (Zn) using concentrated aqueous solutions containing bis(trifluoromethylsulfonyl)amide (Tf_2N^-) anions. An increase in Tf_2N^- concentration significantly enhances water-anion interactions, giving characteristic infrared spectra for the breakdown of the hydrogen-bonding networks of water clusters, *i.e.* loss of free water. For the Tf_2N^- system Zn electrodeposits with the preferred orientation of hcp basal plane was observed, while, for the SO_4^{2-} system with the presence of the hydrogen-bonding networks, preferred orientation of basal plane was not observed. The preferred orientation of basal plane is not attributed to the adsorption of Tf_2N^- anions on the electrode, proved by the use of mixed $Zn(Tf_2N)_2$-$ZnSO_4$ concentrated solutions. The loss of free water in the concentrated $Zn(Tf_2N)_2$ solutions will suppress hydrogen adsorption at the cathode to promote surface diffusion of intermediate Zn^+ adions and growth of Zn crystals. Consequently, the promotions and the easier growth of Zn basal planes with the lowest interfacial free energy will enhance the horizontal growth of Zn basal planes.

Electrochemical reactions in aqueous media are limited by the electrochemical instability of water. This instability involves not only the low voltage of storage batteries but also a limit to metal species electrodeposited from aqueous systems. An effective approach to improve water stability is an increase in solute concentration, *i.e.*, the use of concentrated aqueous solutions.

Although aqueous solutions with extremely high concentrations have been studied for about half a century,[1–4] the attention to highly-concentrated aqueous solutions has revived within this decade. The expansion of the potential window to *ca.* 3.0 V has been reported for a 21 mol kg^{-1} lithium bis(trifluoromethylsulfonyl)amide (LiTf$_2$N, Tf = SO$_2$CF$_3$) aqueous solution.[5] In such concentrated aqueous solutions, the amount of free water is considerably decreased to suppress water electrolysis, which is beneficial for energy storage,[6–11] surface finishing processes,[12–16] and so on. For example, zinc (Zn) electrodeposition from concentrated zinc chloride (ZnCl$_2$) aqueous solutions have demonstrated the suppression of both water decomposition and dendritic growth, which is promising for zinc-air batteries.[9] However, nothing has been studied so far on crystallization mechanisms in concentrated aqueous solutions, *i.e.*, how the decrease in free water affects the crystallization process of electrodeposits is unknown.

Zn electrodeposition thermodynamically competes with hydrogen evolution and/or adsorption because of the relatively negative electrode potential ($Zn^{2+} + 2e = Zn$; $E° = -0.76$ V vs SHE). However, the hydrogen overpotential is large for Zn and the current efficiency is more than 90% even in conventional aqueous solutions with many amounts of free water. In other words, Zn electrodeposition from concentrated aqueous solutions is a good example to examine the effect of a decrease in free water on electrodeposition behaviors because there is no need to take into account the change in current efficiency that affects electrodeposition behaviors.

To identify how the decrease in free water affects Zn electrodeposition behaviors, concentrated aqueous solutions where zinc cations exist as hydrated ions and counter anions are electrochemically stable are desired. In other words, the use of anions is undesirable that coordinate with metal cations and/or are easily reduced. For this reason, we use neither Cl$^-$ anions that coordinate with Zn^{2+},[10,17] nor nitrate (NO_3^-) anions that decompose into nitrite (NO_2^-) anions during cathodic reactions.[18,19] In this study, we report Zn electrodeposition behaviors using concentrated $Zn(Tf_2N)_2$ aqueous solutions. In this system, the hydration of metal cations and the decrease in free water are considered to occur as in concentrated LiTf$_2$N aqueous solutions. For comparison, electrodeposition from concentrated zinc sulfate (SO_4^{2-}) solutions are also studied.

Experimental

***Materials and preparation.***—Zinc sulfate heptahydrates (ZnSO$_4$·7H$_2$O; Nacalai tesque, ≥99.0% purity) was used as purchased. $Zn(Tf_2N)_2$ was synthesized from bis(trifluoromethylsulfonyl)imide (HTf$_2$N; Fluka, ≥95.0% purity) and basic zinc carbonate (2ZnCO$_3$·3Zn(OH)$_2$; Nacalai tesque, chemical pure grade) through acid-base reactions. Their aqueous solutions were prepared with ultra-pure water (18.2 MΩ cm, Millipore, Milli-Q Reference A+). HTf$_2$N (20 mmol) and 2ZnCO$_3$·3Zn(OH)$_2$ (4 mmol) in 20 mL of water were stirred at 500 rpm at 70 °C for 2 h. They were heated at 120 °C for 12 h. to remove excess water. A white, hygroscopic solid was obtained at room temperature. The water amount in this salt was measured by coulometric Karl-Fischer titration. The molalities of ZnSO$_4$ or $Zn(Tf_2N)_2$ solutions were adjusted to 0.1, 0.5, 1.0, 2.0, and 3.5 mol kg^{-1}. We also prepared ZnSO$_4$-$Zn(Tf_2N)_2$ mixed solutions at total Zn^{2+} molality of 2.0 mol kg^{-1}, where molar fractions of $Zn(Tf_2N)_2$, $x = [Zn(Tf_2N)_2]/\{[Zn(Tf_2N)_2] + [ZnSO_4]\}$, were adjusted to be 0.01, 0.10, and 0.20.

Vibration spectroscopy.—For Infrared (IR) measurement, a JASCO FT/IR–460 plus system was used with barium fluoride (BaF$_2$) window materials. For Raman spectroscopy, an integrated Raman system (B&W Tek, innoRam 785)—consisting of a semiconductor laser light source (785 nm), an axial transmissive spectrograph, a holographic probe head, and a CCD detector—was used. For pH measurements, a pH meter (HORIBA, Laquaact D-71) was used.

Electrochemical cells.—Electrochemical measurements were performed at room temperature (RT) using a potentiostat (Bio-Logic Science Instruments, SP-150) by three-electrode method: Cu substrate (YAMAMOTO-MS) as the working electrode (WE), Zn sheet (Nilaco, ≥99.99% purity) as the counter electrode (CE), Ag/AgCl electrode immersed in 3.0 mol dm^{-3} sodium chloride

*Electrochemical Society Member.
zE-mail: kitada.atsushi.3r@kyoto-u.ac.jp
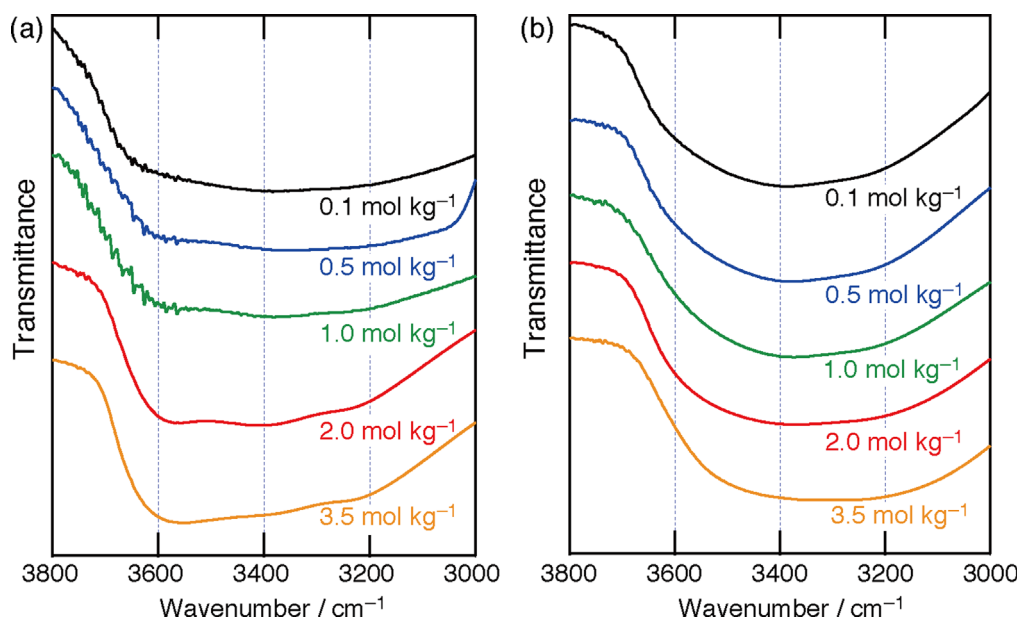
**Figure 1.** IR spectra of O–H stretching vibration modes for (a) $Zn(Tf_2N)_2$ and (b) $ZnSO_4$ solutions.

(NaCl) aqueous solution as the reference electrode (RE). The RE was separated from the main electrolyte by porous Vycor glass. NaCl was used instead of potassium chloride (KCl) to avoid precipitation of less-soluble potassium bis(trifluoromethylsulfonyl) amide (KTf_2N) at the Vycor glass. The potential of the RE is 0.226 ± 0.004 V vs SHE.[20] The liquid junction potential in the RE caused by the difference of ionic mobility between Na^+ cations and Cl^- anions was calculated from Henderson's equation, resulting in below 10 mV. Before the electrochemical measurements, the Cu substrate was ultrasonically cleaned by acetone and ethanol for 20 min. and 10 min., respectively.

Electrochemical measurements.—Linear sweep voltammetry was performed at a scan rate of 10 mV s^{-1}. Prior to linear sweep voltammetry for each electrolyte, the solution resistance was determined by electrochemical impedance spectroscopies at a frequency of 100 kHz and AC voltage amplitude of 20 mV to compensate for the ohmic drop between the WE and the RE.

Electrodeposition and characterization of electrodeposits.— Galvanostatic electrolysis was carried out at a current density of 50 mA cm^{-2} for 400 s without any agitation at RT by the same potentiostat and RE referred before. The thickness of electrodeposits was always *ca.* 10 μm that is thick is enough to eliminate the influence of Cu substrate on Zn electrodeposition, *e.g.* epitaxial growth. To calculate the current efficiency, the weight of the electrodeposits was calculated by comparing the weight of the substrate before and after the electrodeposition. The efficiency was calculated by dividing the weight of the obtained electrodeposits by the weight of the elemental zinc that would be obtained if the current efficiency were 100%. To characterize the electrodeposits, X-ray diffraction (XRD) measurements with $CuK\alpha$ ($\lambda = 0.1542$ nm and scanning electron microscope (SEM) observations were performed using Rigaku RINT2200 and KEYENCE VE-8800, respectively.

Results and Discussion

Infrared spectroscopy.—The presence of free water was examined in $Zn(Tf_2N)_2$ and $ZnSO_4$ solutions with various concentrations. Figure 1 shows the IR spectra of O–H stretching vibration. Broad absorptions ranging from 3000 to 3800 cm^{-1} are observed in 0.1–0.5 mol kg^{-1} $Zn(Tf_2N)_2$ and all $ZnSO_4$ solutions, proving the existence of hydrogen-bonding networks of water clusters.[21] By
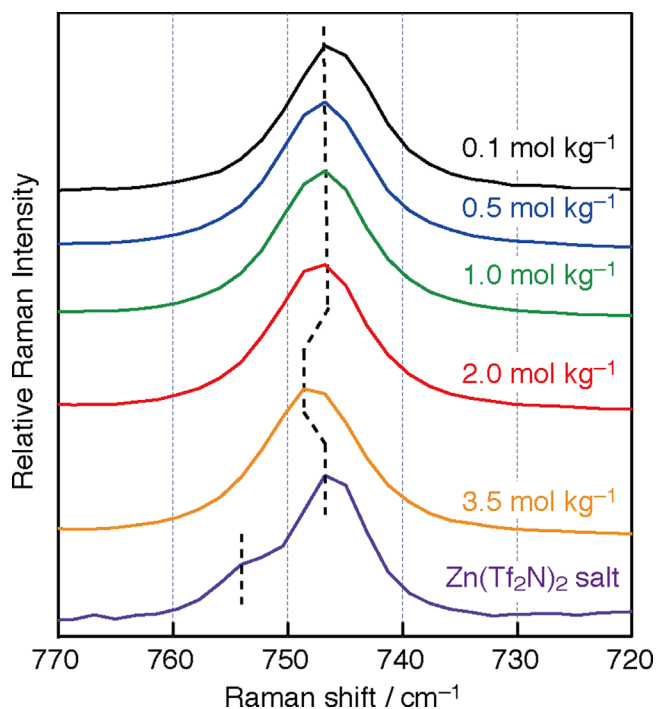
Figure 2. Raman spectra between the Raman shift of 770 and 720 cm^{-1} for 1.0, 2.0, 3.5 mol kg^{-1} $Zn(Tf_2N)_2$ solutions and $Zn(Tf_2N)_2$ solid salt.

contrast, increasing $Zn(Tf_2N)_2$ molality leads to a different situation: The higher shift in O–H vibration ranging from 3200–3500 cm^{-1} to 3500–3700 cm^{-1} indicates that hydrogen-bonding networks of water clusters are broken.

Similar shifts have also been observed in $LiTf_2N$ hydrate melts and concentrated aqueous solutions containing perchlorate (ClO_4^-) anions.[6,22,23] The blue shift at high ClO_4^- concentrations has indicated an increase in the number of water monomers that form hydrogen bonds with ClO_4^- anions.[23] It has been reported that oxygen atoms of the sulfonyl group of Tf_2N^- anions form hydrogen bonds with water molecules.[24] The IR spectra for the concentrated $Zn(Tf_2N)_2$ solutions indicate an increase in the number of water

Table I. pH, Open circuit potentials of the Zn electrode immersed in Zn(Tf₂N)₂ and ZnSO₄ solutions, and the equilibrium potential of Zn²⁺/Zn predicted from the Nernst equation assuming that the activity coefficient of water is 1.

Molality/mol kg⁻¹	pH		Open circuit potential/V vs SHE		Equilibrium potential (predicted)/V vs SHE
	Zn(Tf₂N)₂	ZnSO₄	Zn(Tf₂N)₂	ZnSO₄	
0.1	5.91	5.84	−0.793	−0.807	−0.793
0.5	5.00	5.46	−0.768	−0.796	−0.772
1.0	4.88	5.12	−0.742	−0.787	−0.763
2.0	4.29	5.33	−0.699	−0.770	−0.754
3.5	3.31	3.93	−0.637	−0.742	−0.747

monomer that interacts with Tf₂N⁻ anions. The enhanced water-anion interactions relate to decreasing the amount of free water. Although the amount of free water certainly decreases in ZnSO₄ solutions due to the hydration of Zn²⁺ cations, the amount of free water in Zn(Tf₂N)₂ solutions further decreases by not only the hydration but also the water-anion interactions.

Raman spectroscopy of electrolytes.—Figure 2 shows the Raman spectra of CF₃ bending vibrations of Tf₂N⁻ anions for Zn(Tf₂N)₂ solutions and a Zn(Tf₂N)₂ solid salt. The water content of the solid salt was 5.0 wt%, analyzed by Karl-Fischer titration, which corresponds to the molar ratio Zn(Tf₂N)₂:H₂O = 1:1.8. For the solid salt, a shoulder appears at 754 cm⁻¹ together with the main peak centered at 747 cm⁻¹. In anhydride solid magnesium bis(trifluoromethylsul-fonyl)amide (Mg(Tf₂N)₂) a single Raman band has been observed at 754 cm⁻¹, while a single band has been observed at 750 cm⁻¹ in its hydrate salts (Mg(Tf₂N)₂·8H₂O or [Mg(H₂O)₆][Tf₂N]₂)(H₂O)₂). In other words, the hydration of Mg²⁺ cations has resulted in the shift of the wavenumbers of the CF₃ bending vibrations from 754 cm⁻¹ to 750 cm⁻¹.[25] The shoulder for the solid salt indicates that Zn(Tf₂N)₂ salt with 5.0 wt% H₂O is composed of two phases: anhydride Zn(Tf₂N)₂ salt and its hydrate salts.

By contrast, no shoulder peaks are observed for 0.1–3.5 mol kg⁻¹ Zn(Tf₂N)₂ solutions, indicating that all Zn²⁺ cations are *not* coordinated with Tf₂N⁻ anions but hydrated in the 0.1–3.5 mol kg⁻¹ solutions. A higher shift for the 3.5 mol kg⁻¹ solution indicates the interaction between hydrated Zn²⁺ cations and Tf₂N⁻ anions, similar to the case of concentrated LiTf₂N aqueous solutions.[5] Namely, the Raman spectra for the solutions indicate that Zn²⁺ cations are hydrated without direct inner-sphere complexations where the high Tf₂N⁻ concentration causes the outer-sphere interaction with the hydrated cations.

Open-circuit potentials and prediction of equilibrium potentials.—Table I summarizes the pH values of Zn(Tf₂N)₂ and ZnSO₄ solutions, showing a slight change with solutes and/or concentrations. Table I also summarizes the open-circuit potentials of the Zn electrode immersed in Zn(Tf₂N)₂ and ZnSO₄ solutions. The chemical dissolution of the electrode and hydrogen evolution are not observed during the immersion because Zn(Tf₂N)₂ and ZnSO₄ solutions are both weak acid with pH values more than 3. For this reason, the measured potentials *i.e.*, the mixed potentials are very similar to the equilibrium potential of Zn²⁺/Zn. Compared to the ZnSO₄, the measured potentials for the Zn(Tf₂N)₂ shift toward positive at the same Zn²⁺ concentration. The equilibrium reaction and the Nernst equation are shown in Eqs. 1 and 2, respectively.

$$Zn(H_2O)_6^{2+} + 2e = Zn + 6H_2O \qquad [1]$$
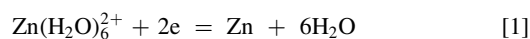
$$E = E° - \frac{RT}{2F} \ln \frac{a_{Zn} a_{H_2O}6}{a_{Zn(H_2O)_6^{2+}}} \qquad [2]$$

where $E°$ and E represent the standard equilibrium potential and the equilibrium potential, respectively, R is gas constant, T is

temperature, F is Faraday constant, and a is the activity. As given in Eq. 1, we assume that Zn²⁺ cations are hydrated by six water molecules.[26]

Table I also shows the equilibrium potentials predicted from the Nernst equation assuming the activity coefficients of solutes and water to be unity. For the ZnSO₄ solutions, the potential values predicted from Eq. 2 are similar to the open-circuit potentials. By contrast, the open-circuit potentials for Zn(Tf₂N)₂ solutions are much more positive than the predicted values because of the significant decrease in water activity. In brief, compared to the ZnSO₄ solutions, increasing Tf₂N⁻ concentration with the enhanced water-anion interactions gives a larger activity coefficient of Zn²⁺ cations and/or smaller water activity, proving that the much decrease in the amount of free water, *i.e.*, loss of free water.

Linear sweep voltammetry.—Figure 3 summarizes linear sweep voltammograms performed on Cu substrate for Zn(Tf₂N)₂ and ZnSO₄ solutions. Note that the voltammograms are compensated for the ohmic drop between the WE and the RE. In Fig. 3, the overpotential is converted from V vs Ag/AgCl immersed in 3.0 mol dm⁻³ NaCl solution to V vs open-circuit potentials of Zn electrode measured in each solution as shown in Table I. Notably, because the measured potentials are very similar to the equilibrium potential of Zn²⁺/Zn as mentioned above, the horizontal axis of this figure is denoted as "Potential/V vs Zn". In all cases, the limiting current density is more than 100 mA cm⁻². The slope of each current–potential curve decreases at a current density of *ca.* 50 mA cm⁻². This decrease may be caused by limited diffusion of hydrated Zn²⁺ cations because hydrogen gas evolution during the cathodic polarization was not detected by eye-inspection. The polarization resistance increases with Zn²⁺ concentration due to enhanced interactions between hydrated Zn²⁺ cation and anion. Compared to the ZnSO₄ solutions, the polarization resistance for the Zn(Tf₂N)₂ solutions is larger at the same Zn²⁺ concentration. The adsorption of Tf₂N⁻ anions on Au substrates has been reported.[27] Similarly, Tf₂N⁻ adsorption will occur on homologous Cu substrate, which may cause an increase in polarization resistance. However, Zn electrodeposition behaviors are affected only by the loss of free water due to concentrating Tf₂N⁻ anions, not by Tf₂N⁻ adsorption on the electrode. This is demonstrated and discussed below.

We also performed cathodic polarization using a Zn²⁺ cation-free LiTf₂N solution with near-neutral pH to investigate Tf₂N⁻ adsorption on Zn substrate. A platinum rod and Ag/AgCl immersed in 3.0 mol dm⁻³ NaCl solution were used as CE and RE, respectively. However, no currents specific to Tf₂N⁻ adsorption on Zn substrate were observed during the polarization.

Electrodeposition from Zn(Tf₂N)₂ and ZnSO₄ solutions.—Flat and smooth electrodeposits were obtained by the galvanostatic electrolysis at a current density of 50 mA cm⁻² using Zn(Tf₂N)₂ and ZnSO₄ solutions. In all cases, the current efficiency was more than 99%, and gas evolution was not detected by eye-inspection. Figure 4 shows the XRD profiles of metallic Zn deposits obtained from each solution. Electrodeposits with the preferential orientation of hcp basal plane, *i.e.* {001} plane, are obtained from the Zn(Tf₂N)₂
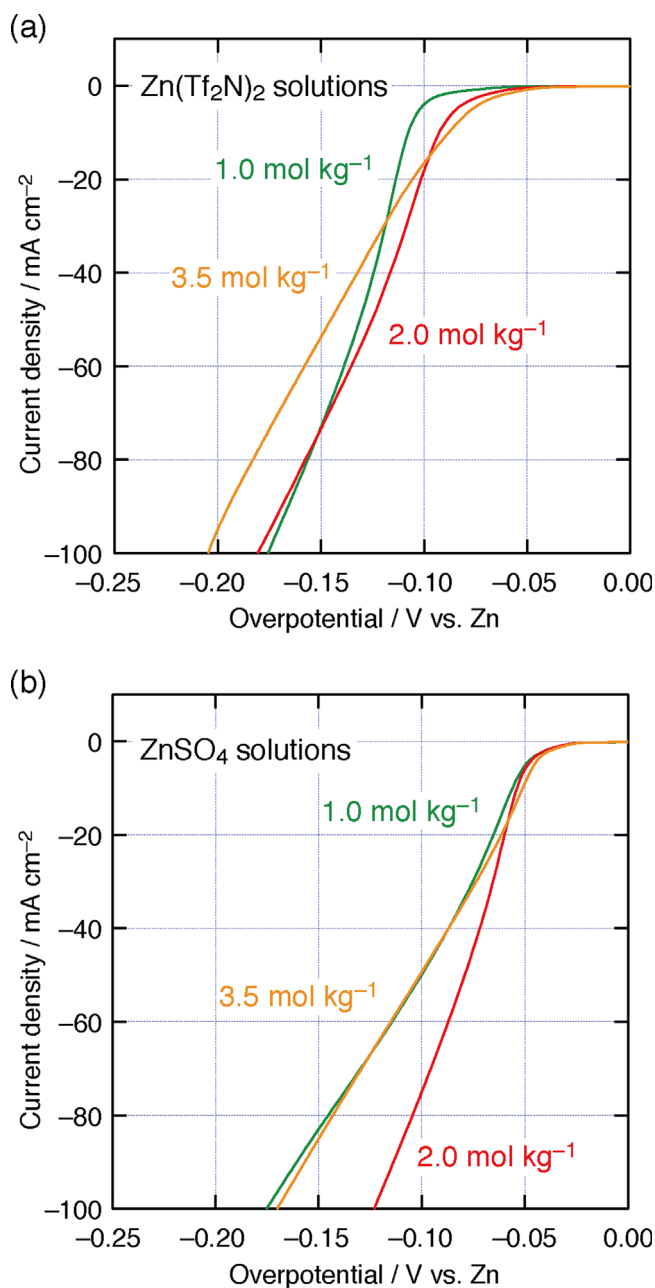
Figure 3. Linear sweep voltammograms with ohmic compensation using Cu substrate at a scan rate of 10 mV s^{-1} for (a) Zn(Tf$_2$N)$_2$ and (b) ZnSO$_4$ solutions.

Figure 4. XRD profiles of Zn electrodeposits obtained from (a) Zn(Tf$_2$N)$_2$ and (b) ZnSO$_4$ solutions. Solid circles and open circles indicate Zn electrodeposits and Cu substrate, respectively.

solutions, and the degree of preferential orientation increases as the concentration decreases down to 1.0 mol kg^{-1}.

In the case of ZnSO$_4$ solutions, such significant basal-plane orientation is not observed and other diffraction intensities associated with hcp pyramidal and/or prismatic planes increase compared to Zn(Tf$_2$N)$_2$ solutions. Figure 5 displays SEM images of the deposits. The anion dependence of the morphology is also proved by the SEM images. Zn deposits with prismatic planes, which have often been reported in Zn electroplating,[28–30] are obtained from the ZnSO$_4$ solutions, while this is not the case with concentrated Zn(Tf$_2$N)$_2$ solutions. Zn deposits for Zn(Tf$_2$N)$_2$ solutions have mossy-like structures. It has been reported that, in the case of zincate baths, mossy-like structures can form on layer-like structures of Zn electrodeposits, *i.e.* on basal planes of Zn.[31,32] Therefore, the fact that mossy-like structures are present only for Zn(Tf$_2$N)$_2$ solutions proves the preferential orientation of hcp basal plane.

The smooth electrodeposits obtained from ZnCl$_2$ hydrate melts have not possessed the preferred orientation of hcp basal planes.[10]

Notably, for 3.5 mol kg^{-1} Zn(Tf$_2$N)$_2$ solutions, the preferred orientation weakens. The degree of cation-anion dissociation decreases compared to the case of 2.0 mol kg^{-1} as shown by the Raman results. Therefore, the weakened preferential orientation for 3.5 mol kg^{-1} Zn(Tf$_2$N)$_2$ solutions may well be attributed to the stronger interaction between hydrated Zn^{2+} cations and Tf$_2$N$^-$ anions. Similarly, an increase in ZnSO$_4$ molality gives a decrease in basal-plane orientation, although the orientation is hardly notable compared to Zn(Tf$_2$N)$_2$ cases. This is related to enhanced interactions between hydrated Zn^{2+} cations and SO$_4^{2-}$ anions as ZnSO$_4$ molality increases. The effects of the enhanced interaction between hydrated Zn^{2+} cations and anions on Zn electrodeposition are discussed below. Below we focus on 2.0 mol kg^{-1} solutions to identify the anion effects on Zn electrodeposition.
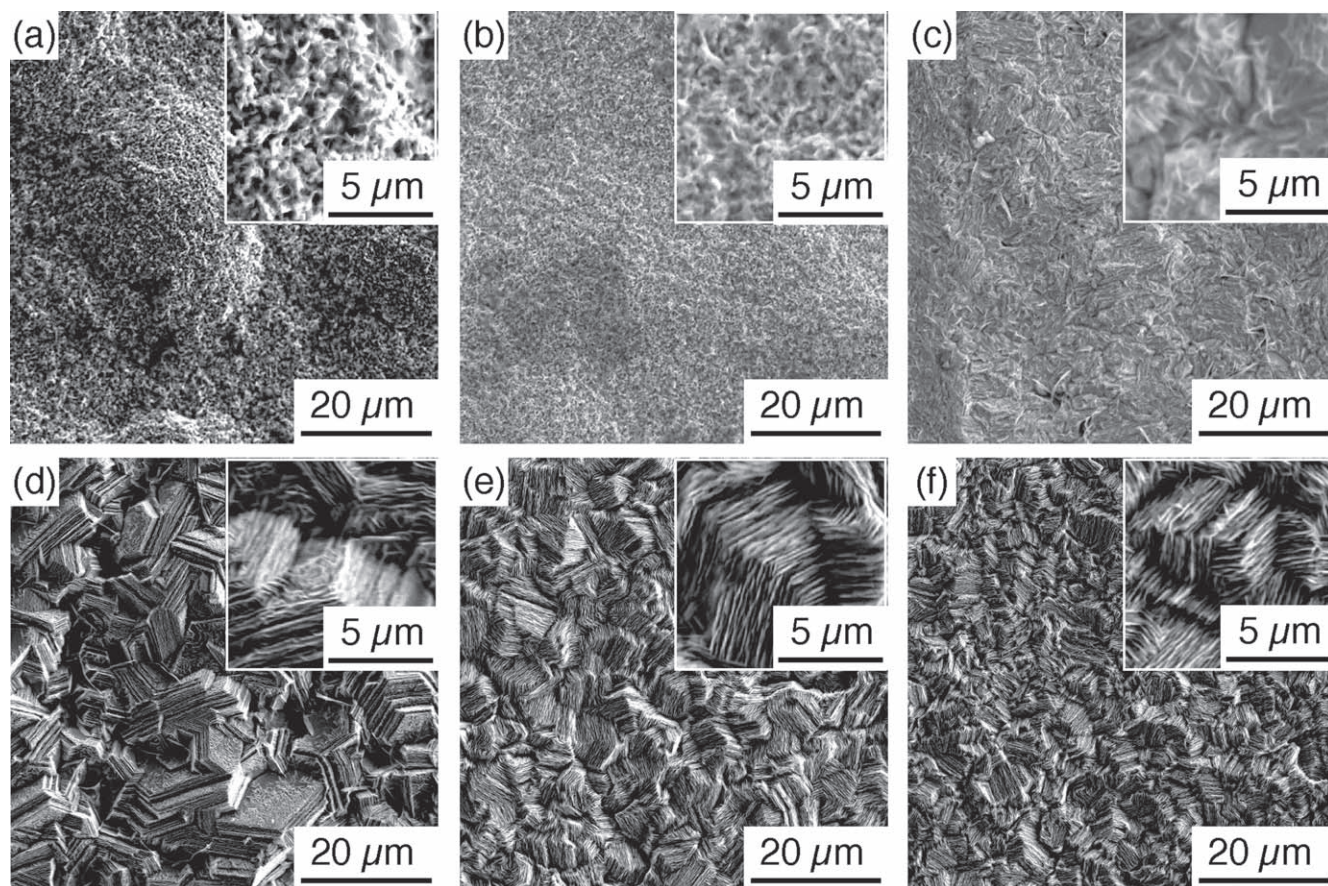
Figure 5. SEM images of Zn electrodeposits obtained from (a)–(c) $Zn(Tf_2N)_2$ and (d)–(f) $ZnSO_4$ solutions, with the molality of (a), (e) 1.0 mol kg^{-1}, (b), (d) 2.0 mol kg^{-1}, and (c), (f) 3.5 mol kg^{-1}. Insets show SEM images with higher magnification.

Identification of the role of Tf_2N^- anions on Zn electrodeposition.—Using mixed $Zn(Tf_2N)_2$-$ZnSO_4$ concentrated aqueous solutions with the total Zn^{2+} concentration of 2.0 mol kg^{-1}, we also performed similar experiments of spectroscopy and electrochemistry, to identify the role of Tf_2N^- anions on Zn electrodeposition.

Figure 6 shows the IR spectra of O–H stretching vibration for the mixed $Zn(Tf_2N)_2$-$ZnSO_4$ solutions. Adding $Zn(Tf_2N)_2$ salt only slightly breaks hydrogen-bonding networks of water clusters, proving that the amount of free water slightly decreases in the mixed solutions. The pH values listed in Table II depend slightly on x or the molar fraction of $Zn(Tf_2N)_2$ ($x = [Zn(Tf_2N)_2]/\{[Zn(Tf_2N)_2]+[ZnSO_4]\}$). Table II also summarizes the open-circuit potentials of the Zn electrode immersed in the mixed solutions. The chemical dissolution of the Zn electrode is not observed during the measurements. Open-circuit potentials gradually shift toward positive with increasing x. Although adding $Zn(Tf_2N)_2$ salt affects the water activity to some extent, these shifts are not significant compared to pure $Zn(Tf_2N)_2$ solutions.

Figure 7 summarizes linear sweep voltammograms for the mixed solutions. Note that the voltammograms are compensated for the ohmic drop between the WE and the RE. In Fig. 7, the overpotential is converted from V vs Ag/AgCl immersed in 3.0 mol dm^{-3} NaCl solution to V vs open-circuit potentials of Zn electrode measured in each solution as shown in Table II. The increase in the polarization resistance with x indicates a stronger inhibition of the electrodeposition by Tf_2N^- adsorption. However, the slope of the voltammogram polarization resistance for pure $Zn(Tf_2N)_2$ solution, *i.e.* $x = 1.00$, after the onset of Zn electrodeposition is similar to that for $x = 0.20$. These results mean that increasing the polarization resistance is attributed to Tf_2N^- adsorption, not to the loss of free water.

For the mixed solutions, electrodeposits obtained by galvanostatic electrolysis at a current density of 50 mA cm^{-2} showed flat and smooth appearances. The current efficiency was more than 99%, and gas evolution was not observed by eye-inspection. Figure 8 shows XRD profiles of the single-phase Zn electrodeposits obtained from the mixed solutions. Basal-plane oriented deposits are *not* obtained from the mixed solutions as in the case of 2.0 mol kg^{-1} $ZnSO_4$ solution. SEM images shown in Fig. 9 also prove that the addition of $Zn(Tf_2N)_2$ salt has almost no effect on the morphologies of Zn electrodeposits.

These results indicate that the only presence of Tf_2N^- anions does not give the preferred orientation of hcp basal planes, although the Tf_2N^- adsorption that increases the polarization resistances occurs. Therefore, the preferred orientation is derived from the loss of free water due to water-anion interactions, not Tf_2N^- adsorption.

Comparison with conventional trends on Zn electrodeposition.—Surface morphologies of metal electrodeposit obtained from aqueous systems have been conventionally controlled by current density, cathodic overpotential, the composition of electrolytes, and additives.[28–30,33–42] The effect of the loss of free water on the morphologies is discussed in comparison to the conventional trends.

Current density and/or cathodic overpotentials have been reported to vary the preferred orientations.[29,30,41,42] Especially in Zn electrodeposition, with increasing the overpotential due to the use of additives and/or the increase in current density, the preferred orientation of hcp basal planes weakens. However, the results of this study differ from this trend. The use of $Zn(Tf_2N)_2$ solutions enhances the preferred orientation of basal planes despite the increased overpotential (see Fig. 4).

Systematic studies exist on the effects of solute concentration, additives, and complexations of metal ions on the microstructure of electrodeposits. As illustrated in Fig. 10,[33–35] five main microstructures have been proposed: field-oriented isolated crystals (FI),
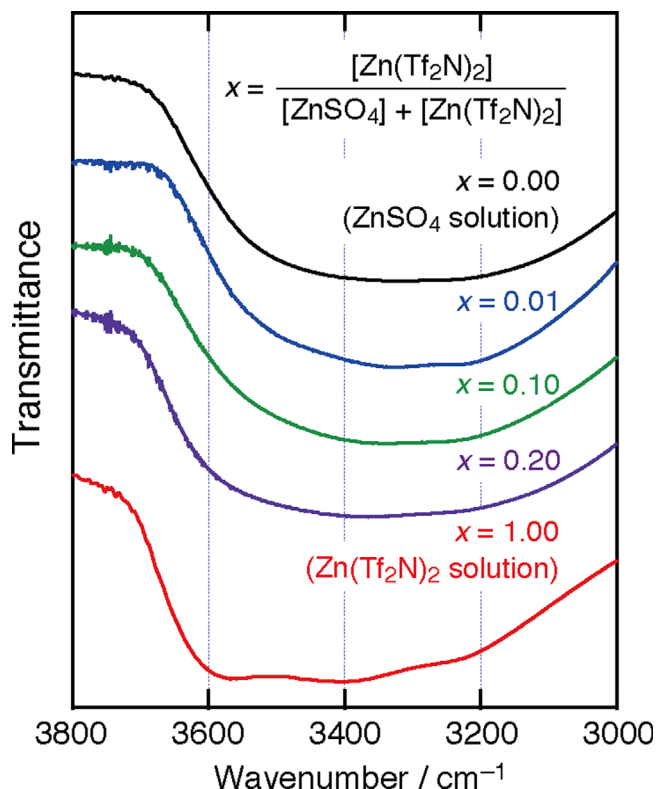
Figure 6. IR spectra of O–H stretching vibration modes for $ZnSO_4$-$Zn(Tf_2N)_2$ mixed solutions with $[Zn^{2+}] = 2.0$ mol kg^{-1}.

Table II. pH values and open circuit potentials of Zn electrode immersed in the mixed solutions with $[Zn^{2+}] = 2.0$ mol kg^{-1}. x indicates molar fractions of $Zn(Tf_2N)_2$, $x = [Zn(Tf_2N)_2]/\{[Zn(Tf_2N)_2] + [ZnSO_4]\}$ in $ZnSO_4$-$Zn(Tf_2N)_2$ mixed solutions at total Zn^{2+} molality of 2.0 mol kg^{-1}.

x	pH	Open circuit potential/V vs SHE
0.00	5.33	−0.770
0.01	4.90	−0.761
0.10	5.13	−0.756
0.20	4.99	−0.745
1.00	4.29	−0.699

basis-orientated reproduction (BR), twining intermediate (Z), field orientated texture (FT), and unoriented dispersion (UD). Inhibition intensity means the difficulty of the electrodeposition reactions due to the use of additives or the complexation of ions. Particularly, in the presence of the complexation, the inhibition intensity increases because the strong interaction between metal cations and ligands prevents the discharge of the complexed ions.

In the conventional trends, the increased inhibition intensity leads to UD. The microstructures for $ZnSO_4$ solutions and the mixed solutions are classified as UD because preferred orientations and epitaxial growth are not observed. For concentrated $Zn(Tf_2N)_2$ solutions, by contrast, the microstructure is classified as FT. To consider whether the loss of free water suppresses the electrodeposition, the change in the microstructure is compared to the growth types shown in Fig. 10, which corresponds to a decrease in the inhibition intensity. This is *not* the case with the use of additives, adsorption of anions and/or the complexation of metal ions. Consequently, the electrodeposition behaviors in the case of loss of free water differ from these conventional trends.
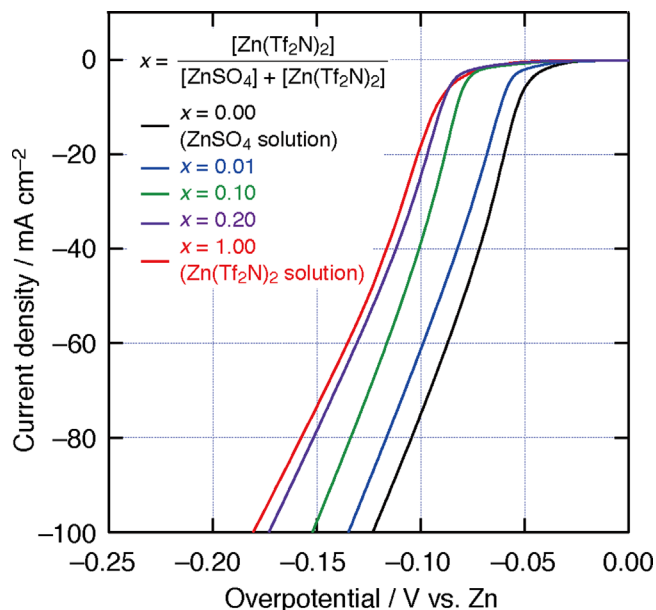

Figure 7. Linear sweep voltammograms with ohmic compensation using Cu substrates at a scan rate of 10 mV s^{-1} for the mixed solutions with $[Zn^{2+}] = 2.0$ mol kg^{-1}.
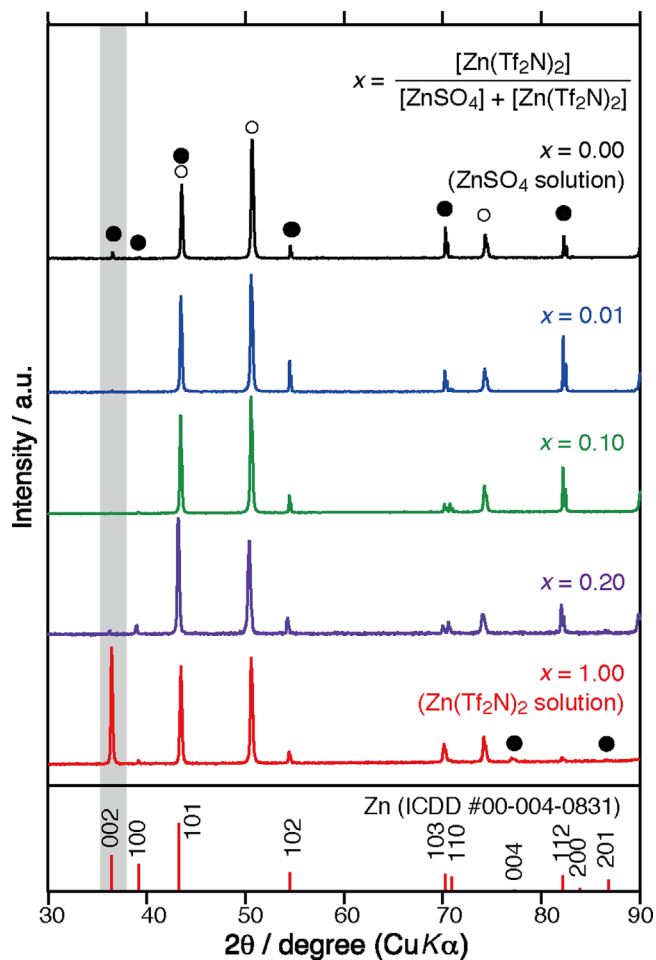
Figure 8. XRD profiles of Zn electrodeposits obtained from mixed solutions with $[Zn^{2+}] = 2.0$ mol kg^{-1}. Solid circles and open circles indicate Zn electrodeposits and Cu substrates, respectively.
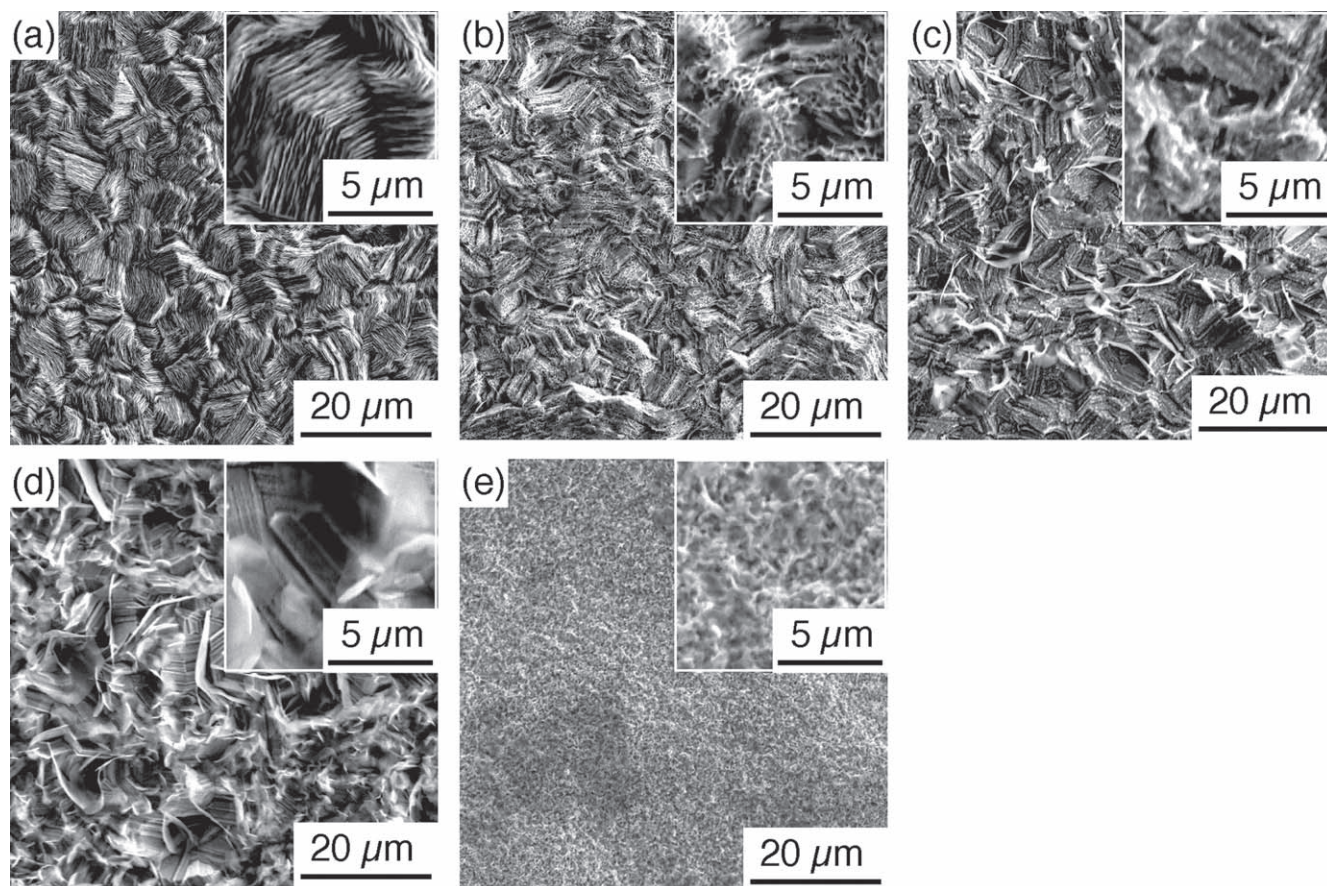
Figure 9. SEM images of Zn electrodeposits obtained from the mixed solutions with $[Zn^{2+}] = 2.0$ mol kg^{-1}; $x =$ (a) 0.00, (b) 0.01, (c) 0.10, (d) 0.20, and (e) 1.00. Insets show SEM images with higher magnification.
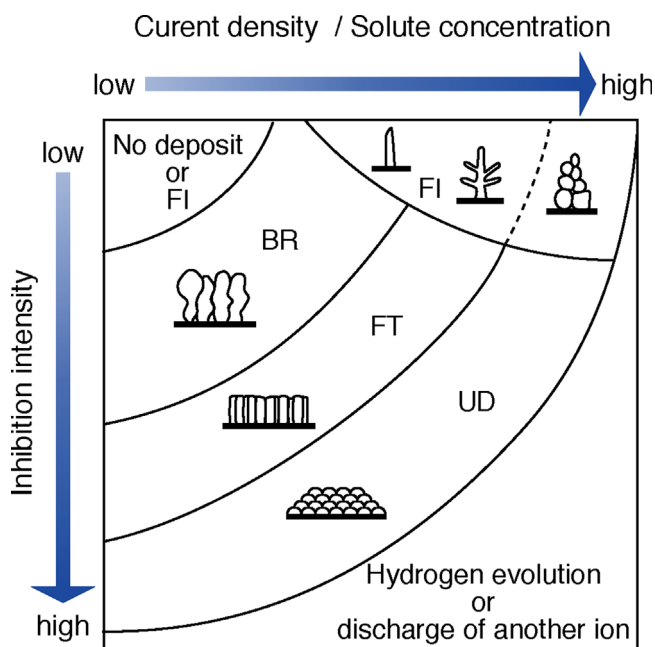

Figure 10. Illustration of an accepted correlation between the microstructure of electrodeposits and conditions, such as current density, solute concentration, and inhibition intensity in conventional aqueous solutions.[33–35]

Notably, in the $Zn(Tf_2N)_2$ and $ZnSO_4$ cases, the enhanced interaction between hydrated Zn^{2+} and anions with increasing solute concentration gives rise to a decrease in the basal-plane orientation as shown in Fig. 4. The decrease in the basal-plane orientation due to the enhanced interaction is related to these conventional trends.[33–35] Similarly to the complexation of ions, the enhanced interactions can inhibit the discharge, although this inhibition is weaker than that in the presence of complexation. In brief, the increase in $Zn(Tf_2N)_2$ or $ZnSO_4$ molality can increase the inhibition intensity and change gradually from the microstructure classified as FT to that as UD. For this reason, increasing $Zn(Tf_2N)_2$ concentration to 3.5 mol kg^{-1} weakens basal-plane orientation as shown in Fig. 4a. Similarly, the $ZnSO_4$ molality gives rise to decrease basal-plane orientation as shown in Fig. 4b, and make smaller the grain size of Zn crystals as shown in Fig. 5.

Effect of loss of free water on Zn electrodeposition.—As mentioned in the Introduction, Zn electrodeposition competes with hydrogen adsorption and/or evolution during cathodic reactions due to the relatively negative electrode potential of Zn. Several investigations have reported that the discharge of Zn^{2+} cations is a two-step reaction involving the formation of intermediate Zn^+ adions and adsorbed hydrogen atoms inhibit the discharge.[43–45] Adsorbed hydrogen has also been suggested to adsorb on active sites for the electrodeposition, such as kink sites.[45] For these reasons, the number of adsorbed hydrogen can affect the nucleation and growth of Zn crystals.

A decrease in the amount of free water by increasing concentrations has been reported to suppress hydrogen evolution due to proton reduction.[14,16] Similarly, hydrogen adsorption due to proton reduction, as well as the hydrogen evolution, can be suppressed in $Zn(Tf_2N)_2$ solutions with a loss of free water compared to $ZnSO_4$ solutions. Besides, the positive shift in open-circuit potentials in $Zn(Tf_2N)_2$ solutions compared to $ZnSO_4$ solutions (see Tables I and II) can decrease contributions of hydrogen evolution/adsorption to competing
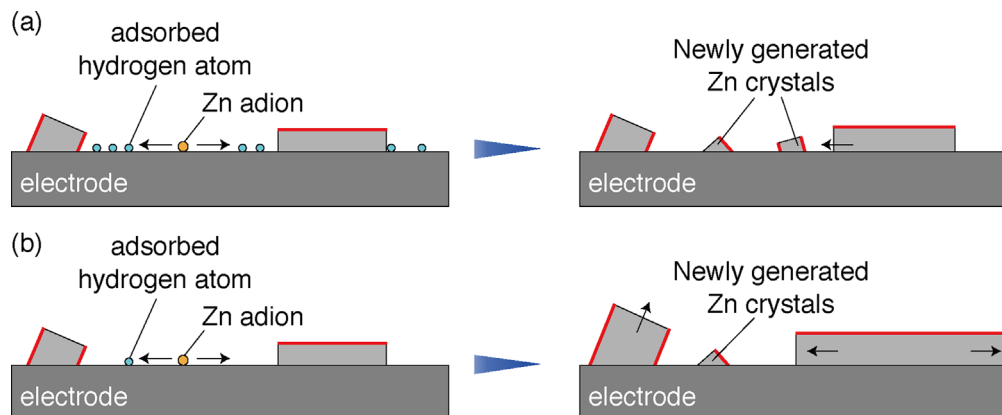
Figure 11. Schematic illustrations of nucleation and/or growth of Zn crystals when the amount of adsorbed hydrogen atoms is (a) large and (b) small. Red lines represent hcp basal planes.

Zn electrodeposition. For these reasons, the number of adsorbed hydrogen atoms will decrease in the concentrated $Zn(Tf_2N)_2$ solutions much more than in the concentrated $ZnSO_4$ solutions despite similar pH values. Notably, even in the $ZnSO_4$ solutions, the number of adsorbed hydrogens is inherently small due to the low strength of the Zn–H bond.[46]

Because the adsorbed hydrogen inhibits surface diffusion of the adions, newly Zn nuclei can be easily generated before the adions diffuse to already existing Zn crystals. Also, hydrogen adsorption on the active sites can inhibit incorporating the adions into the Zn crystals, *i.e.*, the growth of Zn crystals. In other words, the decreased number of adsorbed hydrogen can promote surface diffusion of Zn^+ adions and the growth of Zn crystals. Since the interfacial free energy of basal planes of hcp structure is the lowest, the expansion of basal planes is advantageous for decreasing the interfacial free energy of electrodeposits. For this reason, basal-plane oriented crystals are more geometrically advantageous for the horizontal growth of the electrode than those oriented to other planes.

Figure 11 shows schematic images of the effects of hydrogen adsorption on nucleation and/or growth of Zn crystals. In the case of a large amount of adsorbed hydrogen atoms, surface diffusion of Zn^+ adions and Zn growth will be inhibited by adsorbed hydrogens (see Fig. 11a). For this reason, the horizontal growth of basal-plane oriented crystals will be disadvantageous. By contrast, in the case of few adsorbed hydrogen atoms, there is little geometrical limitation for horizontal growth of basal-plane oriented crystals (see Fig. 11b). Therefore, this easier growth by removing the geometrical limitation can lead to the preferred orientation of basal planes. In other words, by the use of Tf_2N^- anions free water is lost and hydrogen adsorption is suppressed, resulting in the change in Zn electrodeposition behaviors.

The use of concentrated aqueous systems with the suppression of hydrogen adsorption could simplify various industrial processes. One is a baking treatment performed after Zn electroplating on steels. The baking treatment is necessary to remove residual hydrogen atoms in the substrates because this residue causes hydrogen embrittlement and degrades the mechanical properties of the substrates.[47,48] There is a possibility that the use of concentrated aqueous systems decreases the risk of hydrogen embrittlement. We intend to explore this possibility in future studies because the role of reducing the hydrogen adsorption on the mechanical property of Zn electroplated steels is also of interest.

Conclusions

We have investigated the effect of loss of free water on Zn electrodeposition behaviors by the use of concentrated $Zn(Tf_2N)_2$ and $ZnSO_4$ aqueous solutions. Increasing Tf_2N^- concentration enhanced water-anion interactions, giving the breakdown of the hydrogen-bonding networks of water clusters and the loss of free water in stark contrast to the case of $ZnSO_4$ solutions. Hcp basal-plane oriented electrodeposits were obtained only from concentrated $Zn(Tf_2N)_2$ solutions. The use of mixed $Zn(Tf_2N)_2$-$ZnSO_4$ solutions proved that the loss of free water, not Tf_2N^- adsorption, changes the electrodeposition behavior. This change differs from conventional trends of metal electrodeposition using conventional aqueous systems. The loss of free water suppresses hydrogen adsorption on the electrode, giving that surface diffusion of Zn^+ adions and growth of Zn crystals promote. The promotions and the easier growth of Zn basal planes with the lowest interfacial free energy induce the basal-plane oriented electrodeposits.

The use of concentrated aqueous solutions can improve not only the stability of electrolytes in electrochemical devices but also the current electrodeposition processes due to the suppression of hydrogen adsorption. We are confident that this viewpoint will contribute to a deeper understanding of the electrodeposition behaviors of various metals and the improvements of the surface properties of electrodeposits using concentrated aqueous systems.

ORCID

Atsushi Kitada https://orcid.org/0000-0002-4387-8687
Kazuhiro Fukami https://orcid.org/0000-0001-9120-5578
Kuniaki Murase https://orcid.org/0000-0002-7564-9416

References

1. C. A. Angell, *J. Electrochem. Soc.*, **112**, 1224 (1965).
2. C. T. Moynihan, C. R. Smalley, C. A. Angell, and E. J. Sare, *J. Phys. Chem.*, **73**, 2287 (1969).
3. C. A. Angell and J. C. Tucker, *J. Phys. Chem.*, **78**, 278 (1974).
4. S. Deki, M. Ohtawa, and Y. Kanaji, *J. Chem. Soc. Jpn. (in Japanese)*, **12**, 1623 (1979).
5. L. Suo, O. Borodin, T. Gao, M. Olguin, J. Ho, X. Fan, C. Luo, C. Wang, and K. Xu, *Science*, **350**, 938 (2015).
6. Y. Yamada, K. Usui, K. Sodeyama, S. Ko, Y. Tateyama, and A. Yamada, *Nat. Energy*, **1**, 1 (2016).
7. P. Lannelongue, R. Bouchal, E. Mourad, C. Bodin, M. Olarte, S. le Vot, F. Favier, and O. Fontaine, *J. Electrochem. Soc.*, **165**, A657 (2018).
8. W. Deng, X. Wang, C. Liu, C. Li, J. Chen, N. Zhu, R. Li, and M. Xue, *Energy Storage Mater.*, **20**, 373 (2019).
9. F. Wang, O. Borodin, T. Gao, X. Fan, W. Sun, F. Han, A. Faraone, J. A. Dura, K. Xu, and C. Wang, *Nat. Mater.*, **17**, 543 (2018).
10. C. Y. Chen, K. Matsumoto, K. Kubota, R. Hagiwara, and Q. Xu, *Adv. Energy Mater.*, **9**, 1 (2019).
11. N. Zhang, F. Cheng, Y. Liu, Q. Zhao, K. Lei, C. Chen, X. Liu, and J. Chen, *J. Am. Chem. Soc.*, **138**, 12894 (2016).

12. A. Kitada, M. Kurihara, R. Takai, K. Fukami, and K. Murase, *J. Surf. Finish. Soc. Jpn.*, **71**, 376 (2020).
13. K. Adachi, A. Kitada, K. Fukami, and K. Murase, *J. Electrochem. Soc.*, **166**, D409 (2019).
14. K. Adachi, A. Kitada, K. Fukami, and K. Murase, *Electrochim. Acta*, **338**, 135873 (2020).
15. Q. Huang and Y. Hu, *J. Electrochem. Soc.*, **165**, D796 (2018).
16. S. De, J. White, T. Brusuelas, C. Patton, A. Koh, and Q. Huang, *Electrochim. Acta*, **338**, 135852 (2020).
17. S. Peulon and D. Lincot, *J. Electrochem. Soc.*, **145**, 864 (1998).
18. T. Yoshida, D. Komatsu, N. Shimokawa, and H. Minoura, *Thin Solid Films*, **451–452**, 166 (2004).
19. M. Izaki and T. Omi, *J. Electrochem. Soc.*, **144**, L3 (2019).
20. E. A. Ambundo, M. Deydier, A. J. Grall, N. Aguera-Vega, L. T. Dressel, T. H. Cooper, M. J. Heeg, L. A. Ochrymowycz, and D. B. Rorabacher, *Inorg. Chem.*, **38**, 4233 (1999).
21. Z. Wei, Y. Zhang, L. Zhao, J. Liu, and X. Li, *J. Phys. Chem. A*, **109**, 1337 (2005).
22. A. W. Omta, M. F. Kropman, S. Woutersen, and H. J. Bakker, *J. Chem. Phys.*, **119**, 12457 (2003).
23. Y. Chen, Y. Zhang, and L. Zhao, *Phys. Chem. Chem. Phys.*, **6**, 537 (2004).
24. J. K. Clark, S. J. Paddison, M. Eikerling, M. Dupuis, and T. A. Zawodzinski, *J. Phys. Chem. A*, **116**, 1801 (2012).
25. G. Veryasov, U. Harinaga, K. Matsumoto, and R. Hagiwara, *Eur. J. Inorg. Chem.*, **2017**, 1087 (2017).
26. H. Ohtaki, T. Yamaguchi, and M. Maeda, *Bull. Chem. Soc. Jpn.*, **49**, 701 (1976).
27. L. Coustan, G. Shul, and D. Bélanger, *Electrochem. Commun.*, **77**, 89 (2017).
28. K. O. Nayana and T. V. Venkatesha, *J. Electroanal. Chem.*, **663**, 98 (2011).
29. K. Raeissi, A. Saatchi, and M. A. Golozar, *J. Appl. Electrochem.*, **33**, 635 (2003).
30. K. M. Youssef, C. C. Koch, and P. S. Fedkiw, *Electrochim. Acta*, **54**, 677 (2008).
31. T. Mitsuhashi, Y. Ito, Y. Takeuchi, S. Harada, and T. Ujihara, *Thin Solid Films*, **590**, 207 (2015).
32. T. Otani, M. Nagata, Y. Fukunaka, and T. Homma, *Electrochim. Acta*, **206**, 366 (2016).
33. R. Winand, *Mod. Electroplat.* (Wiley, New York) 5th ed., 285 (2011).
34. R. Winand, *Hydrometallurgy*, **29**, 567 (1992).
35. R. Winand, *Electrochim. Acta*, **39**, 1091 (1994).
36. L. Oniciu and L. Mureşan, *J. Appl. Electrochem.*, **21**, 565 (1991).
37. M. C. Li, L. L. Jiang, W. Q. Zhang, Y. H. Qian, S. Z. Luo, and J. N. Shen, *J. Solid State Electrochem.*, **11**, 549 (2007).
38. A. Gomes and M. I. da S. Pereira, *Electrochim. Acta*, **51**, 1342 (2006).
39. M. Mouanga, L. Ricq, J. Douglade, and P. Berçot, *J. Appl. Electrochem.*, **37**, 283 (2007).
40. M. Mouanga, L. Ricq, G. Douglade, J. Douglade, and P. Berçot, *Surf. Coat. Technol.*, **201**, 762 (2006).
41. J. F. S. Filho and V. F. C. Lins, *Surf. Coat. Technol.*, **200**, 2892 (2006).
42. N. A. Pangarov, *J. Electroanal. Chem.*, **9**, 70 (1965).
43. C. Cachet and R. Wiart, *J. Electrochem. Soc.*, **141**, 131 (1994).
44. F. Ganne, C. Cachet, G. Maurin, R. Wiart, E. Chauveau, and J. Petitjean, *J. Appl. Electrochem.*, **30**, 665 (2000).
45. R. Ichino, C. Cachet, and R. Wiart, *Electrochim. Acta*, **41**, 1031 (1996).
46. S. Trasatti, *J. Electroanal. Chem.*, **39**, 163 (1972).
47. K. R. Sriraman, S. Brahimi, J. A. Szpunar, and S. Yue, *J. Appl. Electrochem.*, **43**, 441 (2013).
48. E. M. K. Hillier and M. J. Robinson, *Corros. Sci.*, **46**, 715 (2004).